Three types of bulk impurity induced interference patterns on the (100) and (111) faces of Ne- and Ar-doped silver

Carsten Sprodowski and Karina Morgenstern
Division for Atomic and Molecular Structures (ATMOS), Institute for Solid State Physics, Leibniz University of Hannover, Appelstr. 2, D-30167 Hannover, Germany
(Received 18 June 2010; revised manuscript received 20 August 2010; published 26 October 2010)

Scanning tunneling microscopy and dI/dV mapping reveal three types of interference patterns on Ag(100) and Ag(111) after implantation of argon or neon. These patterns originate from the scattering of bulk electrons between subsurface impurities and the surface. Above nanocavities, the interference pattern develop a rich internal structure. Above point impurities, two types of simpler patterns develop that differ in corrugation, shape, and energy dependence. Low corrugated patterns show a strong dependence on energy, while more corrugated patterns hardly vary with energy. In addition, only the high corrugated patterns reflect the symmetry of the surfaces, while the low corrugated patterns are circular.

DOI: 10.1103/PhysRevB.82.165444 PACS number(s): 68.35.−p, 73.20.−r, 68.37.Ef

I. INTRODUCTION

The electronic structure of the surface determines its interaction with molecules and thus the reactivity of a sample. This electronic structure is homogeneous on a perfect surface but disturbed at point defects or at line defects as step edges or dislocations. Quite recently, it has been shown that subsurface defects also alter the electronic structure of the surface because of the scattering of bulk electrons between them and the surface.[1]

The interference patterns that develop on the surface, when electrons in bulk states are reflected between a subsurface defect and the surface, were measured by scanning tunneling microscopy (STM). These oscillations in the local density-of-states (LDOS) were originally named quantum well states in analogy to the thoroughly investigated quantum well states that develop in thin films.[2] The periodic variation in the density of state at the Fermi level because of a periodic crossing by quantum well states at different film thicknesses was shown indeed to effect a multitude of surface properties, such as chemical reactivity, diffusivity, and thermal stability.[2] A similar influence is also expected for the interference patterns with a similar periodicity as for quantum well states discussed in Refs. 1 and 3–8 and here.

The first observation reported hexagonal interference patterns resulting from argon bubbles below the Al(111) surface.[3] The energy dependence of these Friedel-like oscillations was used by Schmid *et al.* to determine the depth of the bubbles below the surface. On semiconductors, Wittneven *et al.*[4] used the size of circular patterns that develop above ionized dopants to estimate the depth of the dopants. In combination with theory, Schmid *et al.*[5] investigated the Ar related patterns in more detail on both Cu(111) and Cu(100). They could explain those on the former surface by focusing of electron waves in certain crystallographic directions. The almost ringlike features on Cu(100) remained unexplained. In contrast, argon-filled nanocavities below Cu(100) investigated by Kurnosikov *et al.*[6,7] showed pronounced angular variations, which reflected both the shape of the nanocavity as well as an anisotropy of the band structure. Schmid and Kurnosikov established that the Ar filled nanocavities are three dimensional and are limited by low-indexed surfaces by comparing their data to calculations.[5–7] Also above pointlike cobalt impurities angular variations were observed and interpreted by focusing of electron waves in certain crystallographic directions.[1] Again the shape of the interference patterns reflects the underlying band structure of the (111) and (100) faces of copper.[1] The absence of certain features as observed in Refs. 6 and 7 could be explained by different tip-sample distances and/or different tip sharpness.[8]

In this paper, we study interference patterns on Ag(111) and Ag(100). We investigate by scanning tunneling microscopy and scanning tunneling spectroscopy (STS) mapping the electronic signature of interference patterns of different corrugations induced by Ne or Ar implanted below the surface. Three types of patterns are revealed. Patterns above nanocavities reflect the shape of the nanocavities and show a corrugation of up to 20 pm. Patterns above pointlike impurities are either circular with a corrugation of 0.5 pm only or they reflect the symmetry of the surface with a corrugation below 5 pm. The latter patterns can be explained by interference patterns enhanced by focusing effects of the electrons in specific crystallographic directions, while the former are interference patterns without focusing. Our study shows systematically that each of the different patterns discussed in literature within the past decade[1,3–8] can be observed on the same surface.

II. EXPERIMENTAL SECTION

The experiments were performed with a custom-built high-resolution low-temperature STM housed in an ultrahigh-vacuum chamber with a base pressure of $\approx 10^{-10}$ mbar.[9] The STM facilitates measurements with a noise level below 0.5 pm.[10] The single crystalline Ag(111) and Ag(100) surfaces are cleaned by repeated cycles of Ne^+ sputtering with 550 eV and 3 μA for 25 min and annealing at 900 K for 5 min. This is followed by a short cycle of sputtering for 3 min and an annealing for 1.5 min at 800 K.

The surfaces were treated subsequently to different degrees by the following methods. In order to enhance the pattern density, Ne or Ar are implanted into the surface by a

mild sputter pulse (0.4 keV, $I<0.01$ μA, 3 s) with the surface at 100 K, i.e., below the desorption temperature of the noble atoms from the surface (as determined by thermal desorption spectroscopy).

The temperature of sputtering is chosen based on the following reasoning. Ions at the chosen energies are expected to deposit energy into the target via the linear cascade mode.[11] Along the path of the ion through the crystal, vacancy-adatom pairs are produced. Frenkel pairs consist of volume vacancies and interstitials and Schottky pairs consist of volume vacancies and adatoms. Because of material loss into the vacuum some vacancies are unpaired. Only the point defects on the surface can be directly observed by STM. The damage in the bulk has mostly been studied by resistivity measurements on thin foils. These showed that for noble metals as silver, the efficiencies depend rather on the ion energy than on its chemical identity.[12] At the appropriate temperature interstitials migrate.[13] The migration energy is quite low, 70 meV for Ag.[14] Above a threshold temperature, migration increases the number of adatoms observed by STM. This temperature is quite low, e.g., 22 K for platinum for a migration energy of 50 meV.[15] Furthermore, the implanted noble gases migrate and accumulate in agglomeration of vacancies. These structures are called nanocavities[6] as they are limited by low index surfaces.[5] Such nanocavities might thus be filled by the noble gases. Some of them might also be empty as suggested by growth experiment of silver films on Ag(100) at 150 K.[16] Their scattering properties are not expected to be changed measurably by the filling.

Next, the sample is flashed to room temperature or above in order to remove surface adatoms and surface vacancies induced by the sputter pulse. During annealing desorption of the nobel gases is detected by mass spectrometry.

Finally, oxygen molecules, Cu atoms, or Cr atoms are deposited on the sample in order to underline the bulk origin of the patterns. For oxygen deposition, an oxygen pressure of 1×10^{-7} mbar is established in a separately pumped chamber. Molecules are deposited onto the sample by positioning the sample in front of the gate-through valve to this chamber. The valve is opened for 10 s onto the sample mounted on the manipulator and cooled by LN_2 to 110 K. Cr or Cu atoms are deposited from a Knudsen cell onto the sample within the He-cooled shields at 5 K.[17]

STM images are recorded in constant current mode between 5 and 7 K. They are represented in gray scale, whereby brighter corresponds to higher conductivity. STS spectra are taken in open feed-back loop conditions with a sinusoidal modulation voltage of 1 to 4 meV superimposed over the bias voltage and recorded in lock-in technique. dI/dV and d^2I/dV^2 maps are recorded with the same lock-in technique either tuned to the first or second harmonic for dI/dV and d^2I/dV^2 maps, respectively. The height is set by the feed back in the I/V STM image at each pixel of the image. Note that a single map is typically recorded within 80 min not permitting open feed-back conditions during mapping.

Some of the patterns investigated here have a corrugation, which is close to the vertical resolution of the STM of 0.5 pm. Removal of low-frequency noise via fast Fourier transform (FFT) filtering is used on some images to increase the visibility of the features of interest. Apparent heights are determined on the unprocessed images.

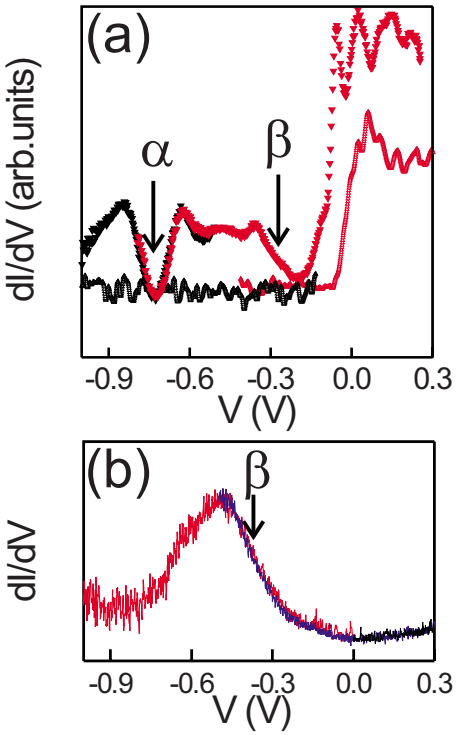

FIG. 1. (Color online) dI/dV spectra; two spectra are superimposed for a larger voltage range: (a) Ag(111); solid symbols: bulk state sensitive tip; open symbols: regular tip; V_{mod}=4 mV at approximately 360 Hz; α and β see text; (b) Ag(100); V_{mod}=1 mV at approximately 380 Hz.

III. RESULTS AND DISCUSSION

A. Details of bulk sensitive tip

We start by explaining shortly the electronic features of a "bulk sensitive" tip. This type of tip is used for the investigation of the interference patterns caused by bulk impurities. The electronic structure of the tip is measured in STS (dI/dV). STS spectra reflect predominantly the local density of states.

The features of the bulk sensitive tip are best explained for a surface that shows an occupied surface state and thus a strong increase in conductivity close to the Fermi energy as does Ag(111). Figure 1(a) shows the dI/dV spectra of the clean Ag(111) surface recorded with a bulk sensitive tip (top spectrum) and a "regular" tip (bottom spectrum). For the regular tip, the most prominent feature is the onset of the surface state at −65 meV. Electrons occupying this surface state and scattered off defects lead to the well-known standing-wave interference patterns observed at bias voltages above the surface state onset,[18–20] also investigated on Ag(111) with the same setup and tip processing as used here.[21,22] An example is shown in Fig. 2(a). The surface state related interference patterns display a typical corrugation of (7 ± 1) pm of the first and 3 pm of the second maximum, when imaged at around 100 meV [Fig. 2(b)]. As these inter-

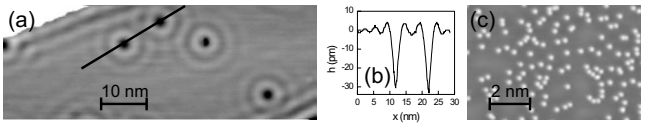

FIG. 2. Surface state related interference patterns on Ag(111): (a) standing wave patterns with a wavelength of 3.8 nm caused by two step edges and five surface impurities, 60 mV, 0.94 nA; (b) line scan as indicated in (a); and (c) STM image with coadsorbed Cu atoms measured below the onset of the surface state; −200 mV, 2 nA.

ference patterns are related to the surface state, they disappear below its onset, even when many impurities are present [Fig. 2(c)].[22] "Regular tips" thus show perfectly flat surfaces on terraces at the same tunneling parameters used below for the investigation of the bulk impurity induced patterns, but surface state standing waves near surface defects above the surface state onset.

Bulk sensitive tips show additional features at larger negative energies (upper spectrum in Fig. 1). This spectrum shows a depression at −725 meV (denoted α), which agrees with a decrease in the density of states in the projected bulk states of Ag(111).[23] Furthermore, the bulk band edge minimum from the $\bar{L}$ point of silver projected onto the (111) surface is observable in this spectrum at ≈−300 meV(β). Also the spectrum of Ag(100) measured with a bulk sensitive tip shows a bulk feature at negative energy [Fig. 1(b)]. The increase in intensity at negative voltage can be related to the pseudo gap of Ag(100) at the $\bar{X}$ point of the surface Brillouin zone that reaches to −400 meV below the Fermi level.[24]

The sensitivity to features of the bulk band structure can be explained by the fact that sharper tips probe a larger region in k space, while blunter tips probe the k space mainly at the $\bar{\Gamma}$ point. As imaging is influenced by the $k_{\|}$ dependent decay into the vacuum, STM images of less sharp tips are expected to give more smeared out patterns or do not show them at all, while sharper tips are sensitive to the bulk interference patterns presented below.

Enhancement in sensitivity to molecular features was achieved before by picking up individual molecules from a surface[25] or by tracking a molecule underneath a tip.[26] This might indicate that not only the shape but also the chemical nature of our bulk sensitive tips is altered. Though the exact nature of the tip is not yet established, we stress that the procedure is very reproducible.

The bulk-sensitive spectrum differs from those usually presented in investigations of surface state properties because in many experiments the tip states are changed by gently bringing tip and surface into contact till all features apart from the surface state onset disappear. A tip modified in this way is usually called a "structure less tip" but should be better named a tip with mainly surface state or $\bar{\Gamma}$ sensitivity (regular tip). In our experiment, we employ the opposite strategy. The tip is changed until it is also sensitive to bulk features, i.e., features away from $\bar{\Gamma}$. We identify a bulk sensitive tip by feature β, which differentiates it clearly from the surface state sensitive tip and is often visible without the fine structure of the spectrum presented in Fig. 1(a). Though not

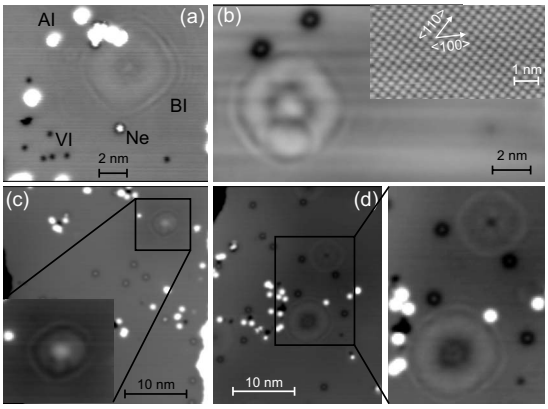

FIG. 3. Overview STM image of Ag(100) after short sputter pulse at 100 K: (a) −195 mV, 1 nA; AI: adatom island, VI: vacancy island, Ne: Neon adatom, BI: bulk interference patterns; (b) 300 mV, 1 nA; inset: atomic resolution image showing the surface orientation, −8 mV, 2.8 nA; (c) −397 mV, 0.96 nA; inset is magnification by a factor of 2 with enhanced contrast; and (d) 195 mV, 0.96 nA with magnification by a factor of 2 with enhanced contrast.

mentioned explicitly, we believe that similar tips were used to investigate the bulk induced interference patterns in the works cited in the Introduction.

B. Formation of bulk related interference patterns

We now demonstrate that implantation of noble gases leads to interference patterns also on silver surfaces. After the short sputter pulse at 100 K there are four different features observed on the Ag(100) surface [Fig. 3(a)]. Clusters of Ag adatoms (white, AI) are found close to impact points of the Ne ion (black, VI) [cf. sputtering defects on Pt(111) (Ref. 15)]. Manipulation experiments show that each of the protrusions contains several adatoms and each of the depressions is a vacancy island consisting of several vacancies. The sombrero shaped protrusions are attributed to single implanted Ne adatoms.[27]

In this paper, we are interested in the more shallow features of much larger diameter [BI in Figs. 3(a) and 3(b)] with a significant radial anisotropy. The same patterns were found after sputtering with argon or neon. They are quadratic with the side of the square along the closed packed direction of the surface [inset in Fig. 3(b)] and a side length between 5 and 8 nm in Fig. 3. They show an apparent height of up to 20 pm. The patterns thus resemble the bulk interference patterns above subsurface nanocavities discussed in the introduction.[3,4,7] From the short wavelength and the characteristic symmetry of the observed patterns we conclude that the patterns result from the scattering of bulk electrons at noble atom nanovacancies. Their bulk origin is corroborated by the fact that the patterns are undisturbed by the adatom clusters and the vacancy islands.

Some further examples are shown in Figs. 3(c) and 3(d). The rings might have a bright or a dark center [cf. Figs. 3(c) and 3(d)] indicative of different depths below the surface.[1] Different patterns are observed at one voltage [Fig. 3(d)] because the nanocavities are neither uniformly sized nor at a

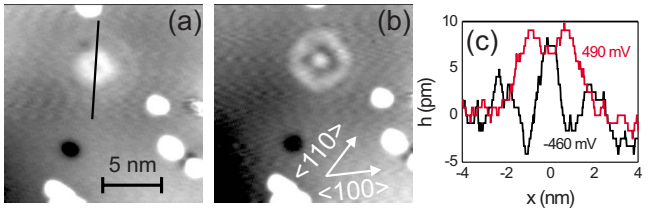

FIG. 4. (Color online) Voltage dependence of interference patterns: (a) 490 mV, 1 nA; (b) −460 mV, 1 nA; and (c) line scans as indicated in (a).

constant depth below the surface.[3] The appearance of the patterns is strongly voltage dependent as demonstrated in Fig. 4. In this particular case the pattern inverses contrast at opposite polarity [Fig. 4(c)]. At +490 mV [Fig. 4(a)] a depression is surrounded by a protruding ring with an apparent height of ≈9 pm followed by another depression and protrusion that are too shallow to be detected in a single line scan. At −460 mV [Fig. 4(b)] a protrusion with an apparent height of ≈7 pm is surrounded by a dark ring followed by another protruding ring of only ≈4 pm in apparent height.

To summarize this part, neon and argon implantation into the surface of Ag(100) leads to interference patterns of up to 20 pm in apparent height due to the formation of nanocavities as observed before for Al(111), Cu(111), and Cu(100).[3,4,7] In the previous work it has been firmly established that the symmetry of these patterns reflect the shape of the nanocavities below the surface that in turn are determined by the symmetry of the planes parallel to the surface. It is thus fourfold symmetric on Ag(100).

C. d^2I/dV^2 maps

As an add-on we propose to investigate these bulk nanocavity related electronic features in future by recording d^2I/dV^2 maps, which reveal further fine structure. Usually d^2I/dV^2 maps are used to show the spatial distribution of molecular vibrations.[30] There, the second derivative of the current enhances the visibility of the small change in conductivity (dI/dV) due to the vibration. Here, the signal is also weak (corrugation of the patterns of 20 pm at most). The second derivative map enhances changes in the conductivity instead of measuring the conductivities as demonstrated in Fig. 5. In the example shown, an additional pattern "B" is observed that is not visible in the I/V images. For this paper it is important that a change of 0.1 V only leads already to visual changes in the patterns observed above nanocavities, e.g., the pattern "C" develops an additional ring at −353 mV.

D. Interference patterns after annealing

Returning to the major topic of this paper, different types of bulk impurity related patterns, we show in Fig. 6(a) that the interference patterns are more uniform after flashing the sample to room temperature or above. Ringlike structures, consisting of a combination of depressions and protrusions, are imaged. The inner circle of varying width is surrounded by at most three maxima/minima, i.e., the patterns exhibit

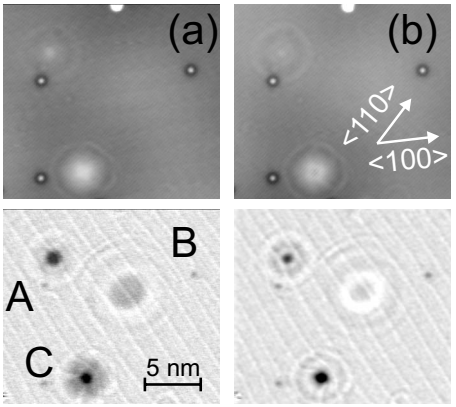

FIG. 5. d^2I/dV^2 maps (bottom row) taken simultaneously with IV images (top row); 3 mV, 632.7 Hz, 1 nA: (a) −453 mV and (b) −353 mV; diagonal stripes in maps are an artifact.

1.5 oscillations. The patterns consist thus of a similar series of depressions and protrusions as the nanocavity related patterns discussed above, but they differ from those in the lack of internal structure and in a lower apparent height of <5 pm. Note that these ringlike patterns are also observed before annealing but are not visible at a contrast that shows the more corrugated patterns.

We observe the same type of ringlike interference patterns on Ag(111) [Fig. 6(b), arrows, and Fig. 6(c)] as on Ag(100). The patterns are presented at a voltage of −200 meV, at which the contribution of the surface state electrons to the formation of the image is small. The corrugation of these patterns is likewise at most 5 pm; the faintest rings visible have a corrugation of less than 0.5 pm at the limit of vertical STM resolution.

The patterns after annealing are more reminiscent of circular features on n-InAs(110) originating from subsurface ionized dopants,[4] i.e., pointlike scatterers, than of those observed above the nanocavities on Cu(100) (Ref. 6) in Figs. 3 and 4. At a specific energy, the inner diameter for a pointlike scatterer is indicative of its depth below the surface and thus variable, while the wavelength should be similar for impurities of different depths.[4] In agreement, we observe that the

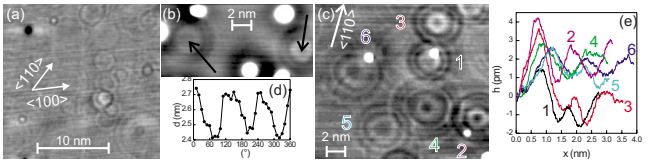

FIG. 6. (Color online) Interference patterns after annealing: (a) STM image of Ag(100); V_{bias}=−45 mV, I_{tunnel}=0.1 nA; a building vibration of a few Hz superimposed over the image was removed by FFT filtering still leading to some "stripes;" (b) STM image of Ag(111), −200 mV, 0.73 nA; arrows point to middle of bulk related interference patterns; white dots are chromium atoms; (c) STM image of Ag(111) for region with more subsurface impurities, but less chromium, −212 mV, 0.56 nA; (d) distance d of black rim measured from center of pattern 5 in (c) in dependence of angle ϕ showing threefold periodicity; and (e) average line scans into 18 different directions from middle of patterns marked by 1 to 6 in (c) with increasing depth below the surface.

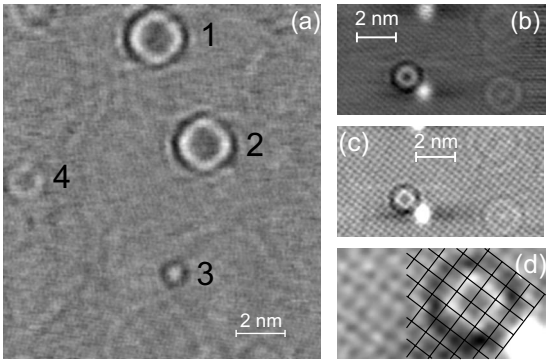

FIG. 7. Interference patterns of different corrugation on Ag(100), white protrusions are coadsorbed oxygen molecules: (a) −28 mV, 7.8 nA; (b) −312 mV, 0.1 nA; (c) −73 mV, 0.1 nA; and (d) zoom-in by factor of 3 on (c) with atomic grid.

diameter of the inner minimum varies largely in Fig. 6(c) between 1 and 3 nm [see Fig. 6(e)], while the distance between the first and the second minimum is with (1.1 ± 0.2) nm almost constant. Similar to Cu(111),[8] the interference patterns on Ag(111) are the larger in their diameter the deeper the defect is buried below the surface because of the pseudo–band-gap in L direction.[8] We thus attribute these interference patterns to standing waves originating from bulk electrons being scattered by a very small subsurface reflector, probably just a point defect similar to the ones observed by Schmid *et al.* also on Cu(100).[5] The bulk origin of these patterns is underlined by the insensitivity of the patterns toward adparticles [chromium on Ag(111), Figs. 6(b) and 6(c)] or molecules [O_2 on Ag(100), Fig. 7(b)]. Note that we are unable to decide, whether these pointlike scatterers are remaining implanted noble gas atoms, Ag atoms at nonlattice sites or single Ag vacancies, or native impurities. The smaller number of these pointlike scatters at higher annealing temperatures rather point against native impurities.

We note that some of the patterns show a considerably stronger corrugation than others, both in Fig. 6(a) on Ag(100) and in Fig. 6(c) on Ag(111), even at a similar size [middle of Fig. 6(a)]. Thereby, the corrugation does not continuously decrease with size as demonstrated in Fig. 7(a). The two quadratically shaped patterns marked "1" and "2" have a side length of 1.64×1.62 nm^2, which corresponds to 4 atoms by 4 atoms. Pattern "3" corresponds to a single atom imaged as a central protrusion and a rim of 8 atoms imaged as depressions. However, pattern "4" is in between these two sizes, but has a lower corrugation of 2 pm than both the larger and the smaller pattern with a corrugation of approximately 4 and 3.5 pm, respectively.

The simultaneous atomic resolution achieved by scanning at low voltage reveals a difference between the rings with different corrugation [Fig. 7(c)]. Three patterns on the right-hand side of the image show much lower corrugation than the one close to the oxygen molecule (white protrusion). For the more corrugated patterns the bright ring coincides with a square of 8 protruding atoms around a single atom and surrounded by 12 atoms of lower apparent height. This pattern is thus fourfold symmetric similar to the ones observed before on Cu(100).[1] In contrast, the other rings are more circular [Fig. 7(b)] and do not show this coincidence, but each ring (depressions or protrusions) is smeared over more than one atomic row.

Also on Ag(111) the more corrugated patterns show deviations from circular symmetry, while the weaker patterns do not. In the STM images this difference is not immediate obvious, so we measured the distance of the rim from the center of the pattern and display one example in Fig. 6(d). The threefold periodicity is then obvious in the sinosoidal distance oscillation with 120. We point out that in Ref. 3 the hexagonal patterns on Al(111) were discussed, but nonhexagonal patterns of much weaker corrugation are visible in Fig. 1 of Ref. 3, though these were not mentioned in the text. The phenomenon is thus not restricted to silver surfaces.

To summarize this part, two different types of patterns are observed after annealing that are attributed to standing waves above pointlike impurities. These patterns differ in corrugation and symmetry.

We now investigate the voltage dependence of the patterns in more detail starting with those of lower corrugation. We concentrate on Ag(100) because of the surface state related patterns superimposed on Ag(111).

E. Voltage dependence of patterns with low corrugation

The quoted apparent heights of the weaker patterns furthermore decrease for larger voltages and are thus too shallow to be quantitatively followed in dependence of their voltage in regular STM images. We therefore present the first derivative, i.e., dI/dV, images. dI/dV maps increase the corrugation because in I/V images all energies from the Fermi energy to the tunneling voltage contribute to the image. In contrast, dI/dV maps record the spatial dependence of the LDOS of the sample within the range of the modulation voltage (typically a few mV to tens of mV).[29]

We present a series of dI/dV maps acquired in the range of occupied states in Fig. 8. In its center, the pattern changes from maximum to minimum and back through this series. The surrounding rings change position in dependence of voltage as best observed in the line scans [Fig. 8(c)]. The most prominent maximum in all of the spectra is found at 0.4 nm at −250 mV and gradually shifts away from the center to 1.2 nm at −850 and −750 mV [Fig. 8(d)]. At −950 mV a maximum is found at 0.8 nm from the center.

A series of dI/dV maps above ionized dopants in InAs(110) in the voltage range from 50 to 175 meV showed a monotonous decrease in the rings with increasing voltage. This does not contradict our result in view of the different voltage ranges.

The position of the maxima at different energies can be explained by the fact that electrons of different energies form standing waves at different distances between the subsurface impurity and the surface. As the vertical distance is fixed by the position of the subsurface impurity, the standing waves are observed at different angles. The maximum at −950 mV at lower distance than those at −850 or −750 mV might indicate a phase flip induced by a resonance. We thus summarize that the circular patterns of low corrugation show a considerable change in position of the maxima and minima

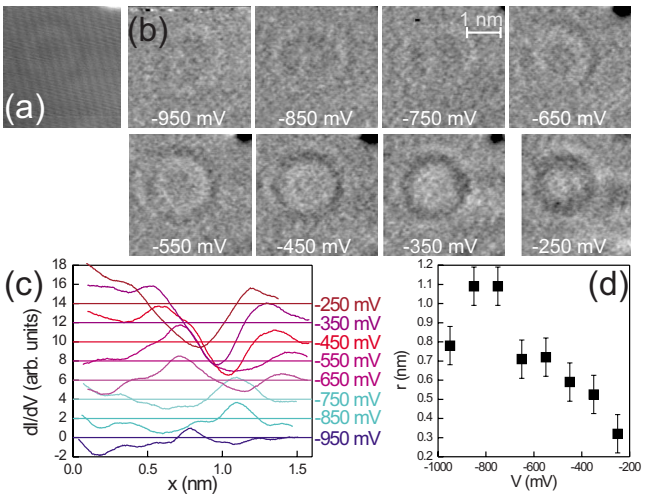

FIG. 8. (Color online) dI/dV maps on interference patterns at indicated voltage: (a) I/V image at 350 mV, 1 nA; (b) dI/dV map at indicated voltages, V_{mod}=2 mV, 383.3 Hz; (c) line scans of dI/dV map; average of 16 line scans from middle of structure in 16 different angular directions; shifted by 2 in y; horizontal line represent average signal on surface for indicated voltage; and (d) position of first maximum from center in dependence of voltage as extracted from (b).

by several tenths of nanometer within a voltage range of several 100 mV.

F. Current and voltage dependence of more corrugated patterns

The patterns with higher corrugation show a much smaller, if any, dependence on voltage. The pattern in Fig. 9(a) shows a decrease in corrugation but no other visual change within two orders of magnitude in voltage. Measurement of the size of the white and black ring, respectively, show a change of 0.2 nm only within this voltage range [Fig. 9(b)].

A larger ring of high corrugation is investigated in the hundred mV range. A line scan of the quadratically shaped rings in Fig. 7 is shown in Fig. 9(c). The average size of its inner protruding ring is approximately 1.7 nm in [100] and the corrugation of less than 3 pm at −16 mV and 0.5 nA. The diameter of the white ring does not change measurably in the voltage range down to −300 mV. Note that during this type of measurement the tip-sample distance is not constant. In general the patterns are expected to change with tip distance to the surface because of the different k-parallel selections, i.e., the different exponential decay of different electronic states into the vacuum. Up to ≈8 nA, only the corrugation decreases with smaller currents and the lateral dimension of the protrusion does not change [within the experimental uncertainty, Fig. 9(e)]. However, it should be kept in mind that a change in the current by one decade corresponds to a change in tip-sample distance by approximately 0.1 nm only.

In order to exclude any compensation effects, we determine the dependence on voltage at (almost) constant tip-sample distance [Fig. 9] between −500 and +500 mV by

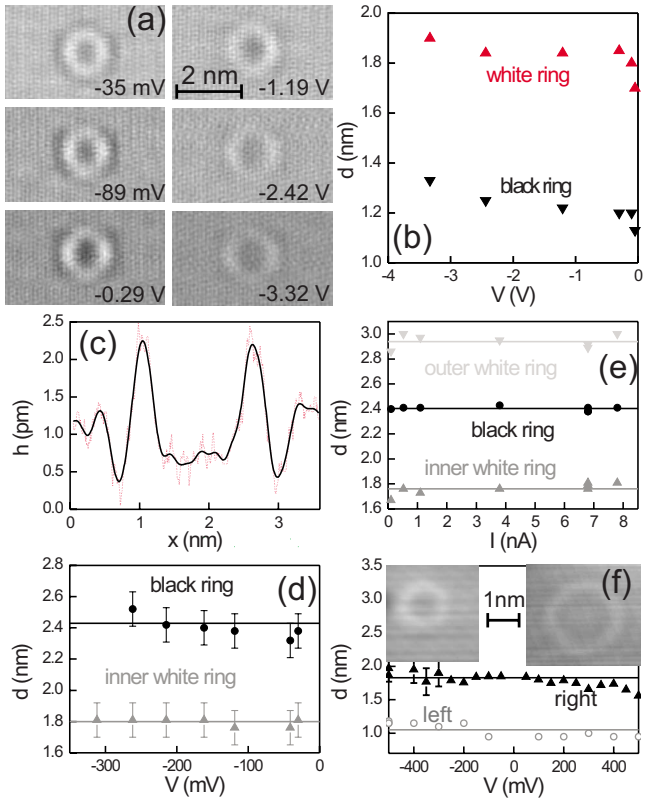

FIG. 9. (Color online) Current and voltage dependence of more corrugated interference patterns on Ag(100): (a) STM images at different voltage as indicated, 43 pA, 6.8 K; (b) voltage dependence of (a) (large voltage range); (c) line scan across upper square in Fig. 7(a) at −16 mV and 0.5 nA; (d) and (e) average size d (measured in direction of fast scanning, i.e., [100]) of (c) in dependence of current at −18 mV (d) and of voltage V at 6.8 nA; lines are average values; and (f) average size d in dependence of voltage V at constant tip-sample distance for white rings shown in insets; error bars are representative.

adjusting the tunneling current at each voltage according to standard tunneling theory. This experiment confirms that there is a very weak, if any, voltage dependence of the patterns of higher corrugation. This is clearly different from the voltage dependence of the two other patterns discussed above.

The shape, higher corrugation, and weak voltage dependence can be explained by focusing effects.[8] Electrons scattered at pointlike defects do not propagate in a spherical wave as in free space but are focused in preferential directions because of deviations of the silver Fermi surface from a spherical shape similar to the one of Cu.[1] This leads to a preferred propagation of the bulk electrons in narrowly confined directions. The maximum constructive interference occurs in the direction normal to the Fermi surface. In agreement with the symmetry of the fcc Brillouin zone in [111] direction and in [100] of the surface this deviation is threefold for Ag(111) [Fig. 6(b)–6(d)] (Ref. 28) and fourfold for Ag(100) (Fig. 7).

The focusing cone intersection with the surface is imaged in STM. The enhanced corrugation of these patterns results from the fact that focused electrons are hardly damped and

thus detectable at much larger distances from the source than nonfocused electrons.[8] The size of the Fermi surface of Ag is close to the extension of the first Brillouin zone. In some directions the Fermi wave vector even reaches the zone boundary. This implies that the wavelength $\frac{\pi}{k_F}$ of the LDOS oscillations is only slightly larger than the interatomic distances. The focused electrons may thus travel (almost) along low indexed directions of the bulk if the point impurity substitutes a crystal atom. It thus coincides with atomic rows of the surface. Whether or not additional effects as e.g., atomic relaxation due to a changed electronic structure, enhance the visibility of the patterns in STM could be solved by theoretical calculations, which we hope to induce by this paper.

IV. CONCLUSION

In this paper, we demonstrated that three types of bulk impurity related interference patterns might be observed by high-resolution scanning tunneling microscopy with a bulk-sensitive tip. Above nanocavities the patterns are complex and change substantially for small changes in the voltage. Many different shapes are observed as these patterns reflect also the shape of the nanocavity. The observed dispersion might indicate that focusing effects are not dominant in formation of this pattern. Focusing might be hindered by the possible distortion of the lattice close to the nanocavity. Above pointlike scatterers two less complex patterns are observed consisting of simple rings. Low corrugated patterns of circular shape show strong dispersion, while higher corrugated ones with distinct symmetry of the surface show little, if any, dispersion. The low corrugated patterns are explained as a simply standing wave between the subsurface impurity and the surface. For the higher corrugated patterns, in addition focusing of the electrons in specific crystallographic directions as discussed in Refs. 1 and 5 leads to an enhancement of the changes in specific rows of atoms. The three patterns thus alter the electronic structure at the surface differently. A possible explanation for scattering is the position of the impurity, which might be interstitial or substitutional.

The local variation in electronic structure of the surface will influence processes on surfaces as nucleation or reactivity. Nucleation might be influenced by a change in adatom diffusivity or by providing specific nucleation centers. We observe, for example, that the three chromium atoms in Fig. 6(c) are adsorbed in the maxima of the interference patterns. Likewise the reactivity of surface is expected to be altered locally. As a corollary, we suggest to investigate these type of low corrugation patterns in dI/dV or even d^2I/dV^2 maps, which enhances differences at different energies.

ACKNOWLEDGMENTS

We acknowledge financial support by the Deutsche Forschungsgemeinschaft. We gratefully acknowledge Michael Mehlhorn for experimental support and Christopher Zaum for performing the TDS spectra. We thank Martin Wenderoth, University of Göttingen, and Stefan Blügel, Forschungszentrum Jülich, for fruitful discussions and critical reading of this paper.

[1] A. Weismann, M. Wenderoth, S. Lounis, P. Zahn, N. Quaas, R. G. Ulbrich, P. H. Dederichs, and S. Blügel, Science **323**, 1190 (2009).
[2] A. L. Vázquez de Parga, J. J. Hinarejos, F. Calleja, J. Camarero, R. Otero, and R. Miranda, Surf. Sci. **603**, 1389 (2009).
[3] M. Schmid, W. Hebenstreit, P. Varga, and S. Crampin, Phys. Rev. Lett. **76**, 2298 (1996).
[4] C. Wittneven, R. Dombrowski, M. Morgenstern, and R. Wiesendanger, Phys. Rev. Lett. **81**, 5616 (1998).
[5] M. Schmid, S. Crampin, and P. Varga, J. Electron Spectrosc. Relat. Phenom. **109**, 71 (2000).
[6] O. Kurnosikov, O. A. O. Adam, H. J. M. Swagten, W. J. M. de Jonge, and B. Koopmans, Phys. Rev. B **77**, 125429 (2008).
[7] O. Kurnosikov, J. H. Nietsch, M. Sicot, H. J. M. Swagten, and B. Koopmans, Phys. Rev. Lett. **102**, 066101 (2009).
[8] A. Weismann, Ph.D. thesis, Universität Göttingen, 2008.
[9] M. Mehlhorn, H. Gawronski, L. Nedelmann, A. Grujic, and K. Morgenstern, Rev. Sci. Instrum. **78**, 033905 (2007).
[10] M. Mehlhorn and K. Morgenstern, Phys. Rev. Lett. **99**, 246101 (2007).
[11] *Sputtering by Particle Bombardement I*, edited by R. Behrisch (Springer, New York, 1981).
[12] R. S. Averback, R. Benedek, and K. L. Merkle, Phys. Rev. B **18**, 4156 (1978).
[13] J. M. Rojo and L. Bru, Philos. Mag. **25**, 1409 (1972).
[14] N. Q. Lam, L. Dagens, and N. V. Doan, J. Phys. F: Met. Phys. **13**, 2503 (1983).
[15] M. Morgenstern, Th. Michely, and G. Comsa, Phys. Rev. Lett. **79**, 1305 (1997).
[16] C. Kim, R. Feng, E. H. Conrad, and P. F. Miceli, Appl. Phys. Lett. **91**, 093131 (2007).
[17] Note that the identity of the adparticle is not of importance to the results presented here and we used whatever was present in the UHV chamber from separate experiments. As the results presented in this article were acquired over the course of several years several different adparticle were used.
[18] M. F. Crommie, C. P. Lutz, and D. M. Eigler, Nature (London) **363**, 524 (1993).
[19] M. F. Crommie, C. P. Lutz, and D. M. Eigler, Science **262**, 218 (1993).
[20] Ph. Avouris and I.-W. Lyo, Science **264**, 942 (1994).
[21] K. Morgenstern, K. F. Braun, and K. H. Rieder, Phys. Rev. Lett. **89**, 226801 (2002).
[22] K. Morgenstern, K. H. Rieder, and G. A. Fiete, Phys. Rev. B **71**, 155413 (2005).
[23] St. Huefner, *Photoelectron Spectroscopy*, 2nd ed. (Springer, Berlin, 1996), p. 382.
[24] B. Reihl, K. H. Frank, and R. R. Schlittler, Phys. Rev. B **30**, 7328 (1984).
[25] L. Bartels, G. Meyer, and K. H. Rieder, Appl. Phys. Lett. **71**,

213 (1997).
[26] M. Böhringer, K. Morgenstern, W.-D. Schneider, and R. Berndt, Surf. Sci. **457**, 37 (2000).
[27] This is supported by three observations. First, the sombrero shaped protrusions are not observed when sputtering with Argon. Second, adsorbed Ne adatoms are imaged as a simple protrusion with a higher apparent height at similar tunneling parameters. Third, these adsorbed Ne adatoms are such vulnerable to the scanning process that they can only be imaged, if attached to defects in contrast to the sombrero shaped feature observed here.
[28] As simultaneous atomic resolution requires imaging above the surface state onset, we were not able to achieve it on Ag(111) simultaneously with the bulk features and thus a row of protruding atoms could not be resolved.
[29] M. Ziegler, N. Neel, A. Sperl, J. Kröger, and R. Berndt, Phys. Rev. B **80**, 125402 (2009).
[30] W. Ho, J. Chem. Phys. **117**, 11033 (2002).